Adsorption of arsenate, phosphate and humic acids onto acicular goethite nanoparticles recovered from acid mine drainage

Adsorption of arsenate, phosphate and humic acids onto acicular goethite nanoparticles recovered from acid mine drainage

Regina F.P.M. Moreira[1], Solange Vandresen[1], Danielle B. Luiz[1], Humberto J. José[1] , and Gianluca Li Puma[2]

[1]Department of Chemical Engineering and Food Engineering (EQA), Laboratory of Energy and the Environment (LEMA), Federal University of Santa Catarina (UFSC), Campus Universitário, Trindade, CP 476, Florianópolis - Santa Catarina, 88040-900, Brazil .

[2] Environmental Nanocatalysis & Photoreaction Engineering, Department of Chemical Engineering, Loughborough University, Loughborough LE11 3TU, United Kingdom

*Corresponding author: Department of Chemical Engineering and Food Engineering, Federal University of Santa Catarina, Campus Universitário, Trindade, PO box 476, Florianópolis – SC, 88040-900, Brazil. Phone: +55 48 3721-2536; Fax: +55 48 3721-9687. E-mail: regina.moreira@ufsc.br

Abstract

Acicular goethite nanoparticles (AGNs), obtained from the active treatment of acid mine drainage (AMD) on an industrial scale, were evaluated with respect to their capacity to adsorb the contaminants arsenate, phosphate and humic acids (HAs) in aqueous solution. Kinetics and equilibrium constants that describe the adsorption process were investigated. The adsorption capacity decreased in the order: HAs (37 mgC g^{-1}) > As(V) (20 mg As(V) g^{-1}) > phosphate ions (13 mgPO_4^{3-} g^{-1}). The adsorption capacity of the AGNs produced from acid mine drainage to remove arsenate, phosphate or humic acids are similar to those found for other synthetic iron oxides produced under controlled conditions at the laboratory scale. This study demonstrates the valorization of the AGNs product derived from acid mine drainage slurry waste arising from the mining of coal as an effective adsorbent materials for water treatment.

Keywords: iron oxides, adsorption, water treatment

Nomenclature

AGN: acicular goethite nanoparticles

AMD: acid mine drainage

k_1 (min^{-1}) and k_2 (g mg^{-1} min^{-1}): adsorption rate constants of pseudo-first and pseudo-second order

K_F, n (dimensionless): Freundlich parameters

q_t: amount adsorbed at time t (mg g^{-1})

q_e: amount adsorbed at equilibrium (mg g^{-1})

q_m: monolayer adsorption capacity (mg g^{-1})

b: Langmuir constant (L mg^{-1})

BET: Brunauer-Emmett-Teller method

BJH: Barret-Joyner-Hallenda method

ST: Saito-Foley method

C: concentration of adsorbate at equilibrium (mg L^{-1})

Co: initial concentrations of adsorbate (mg L^{-1})

EDS: energy dispersive X-ray spectrometer

HAs: humic acids

pH_{pzc}: point of zero charge

SEM: scanning electron microscopy

V: initial volume of adsorbate solution (L)

w: mass of adsorbent (g)

C_o and C_e: concentrations of adsorbate - initial and at equilibrium, respectively (mg L^{-1});

1. Introduction

Acid mine drainage (AMD) arising from the mining of metals or coal, represents a serious environmental problem when left uncollected and untreated. Typically, in Brazil, each ton of coal produces 2.5 m^3 of AMD, which contains 2 to 15 g L^{-1} of iron [1]. AMD causes the degradation of surface and ground waters, soils and sediments, and poses a serious hazard to aquatic biota and to humans. AMD is formed when sulfide minerals, predominantly pyrite (FeS_2) but also arsenopyrite (FeAsS), chalcopyrite ($CuFeS_2$) and chalcocite (Cu_2S), among others, are exposed to oxygen and water, causing an oxidation reaction that produces sulfuric acid (H_2SO_4). The waters are characterized by a low pH and high concentrations of iron, and often, other metals and toxic chemicals such as SO_4^{2-}, CO_3^{2-}, Al^{3+}, Mn^{2+}, Zn^{2+}, Cu^{2+}, Ni^{2+}, Ca^{2+}, Mg^{2+}, Cr^{3+}, As^{3+}, As^{5+}, Pb^{2+}, cadmium and mercury. Futhermore, naturally

67 occurring bacteria such as *Acidithiobacillus ferrooxidans* can accelerate AMD production
68 considerably [2, 3].

69 As a result of the gravity of the environemntal damage that AMD poses, new
70 emerging methods for the treatment of AMD have been investigated, including the use of
71 fly-ash zeolite, fuel cell technologies, peat-humic agent, microfiltration and electrodialysis
72 [2,4-6], besides the traditional method of remediation involving alkaline neutralizing agents
73 such as anhydrous ammonia, hydrated lime, sodium hydroxide, sodium carbonate and
74 limestone, which cause the precipitation of the heavy metals in the AMD in the form of
75 hydroxides and/or oxides sludge [7]. In parallel, potential applications for the recovered
76 AMD sludge are currently being sought, such as its use as pigments [8] and as adsorbent
77 materials [9 – 11].

78 The application of iron oxides or hydroxides as adsorbents for the removal of water
79 contaminants is well documented, however, it is desirable to develop greener and low cost
80 sources of iron, reusing industrial waste rich in iron, thus avoiding the synthesis of iron
81 adsorbents from analytical-grade chemicals [12].

82 Our research group has recently demonstrated the production of acicular goethite
83 nanoparticles (AGNs) from AMD on an industrial scale [1]. In this process, 60 m^3 h^{-1} of
84 AMD collected from a coal mine in the southern state of Santa Catarina (Brazil) was treated,
85 generating a chemical sludge at a flow rate of 4-35 tonn day^{-1} with the percentage of iron
86 oxides being greater than 80%. The iron oxide production consists of four steps: (1)
87 neutralization by adding $Ca(OH)_2$ until reaching pH 3.8, followed by the settling of
88 aluminum hydroxide and calcium sulfate; (2) neutralization with NaOH and precipitation
89 of $Fe(OH)_2$; (3) slow oxidation of $Fe(OH)_2$; (4) thermal treatment at temperatures in the
90 range of 100–700 °C. [13, 14]. The valorization and reuse of this sludge has been

investigated for the preparation of oxidation catalysts for the oxidation of volatile organic compounds, for the production of pigmental dyes and for the removal of metal ions [13, 14]. In this study, we evaluate a new application of acicular goethite nanoparticles (AGNs), which is produced from the treatment of 60 m^3 per day AMD and at high purity (> 80%), as adsorbent for environmental remediation of water contaminated with arsenate, phosphate and humic acids. This is in response to strict limits of 10 $\mu g.L^{-1}$ on arsenic in drinking water dictated by the US Environmental Protection Agency, the World Health Organization (WHO) and the European Commission. Arsenic is an environmental contaminant associated with the highest risks of morbidity and mortality worldwide, both because of its toxicity and the number of people exposed [15] and dangerously high levels of arsenic have been identified in many water supplies around the world [16]. Excess phosphorous is associated with algal blooms events, which can cause high economic damage in coastal oceans and lakes [17], in addition to the formation of extremely toxic species in drinking water [18]. Sewage and urban wastewaters commonly contain 10–30 mg L^{-1} of phosphate ions and biological and physico-chemical treatments are the most commonly used methods for their removal. Although widely applied, these methods have disadvantages including excessive sludge production, high chemical demand and difficulty in achieving regulatory guideline levels, since only 75% to 85% of the phosphate is typically removed. These problems are not encountered when adsorption methods are used [19]. Finally, color-causing humic substances have long been a problem for the water supply industry, since trihalomethanes (THMs), haloacetic acids (HAAs) and other halogenated organic compounds can be formed during the chlorination of water supplies [20]. These problems highlight the need to remove these compounds from water and wastewaters.

2. Materials and methods

2.1 AGN recovery from AMD

The chemical sludge was obtained from the treatment of AMD at a coal mine located in the state of Santa Catarina in southern Brazil. The adsorbent was prepared from the AMD following the protocol described in Madeira [18]. Briefly, the active treatment consists of an AMD (pH 2.5; $[Fe^{2+}]$ = 2.5 g L^{-1}; $[SO_4^{2-}]$ = 9.0 g L^{-1}; $[Al^{3+}]$ = 33.5 mg L^{-1}; $[Mn^{2+}]$ = 72.4 mg L^{-1}) pre-neutralization step with lime ($Ca(OH)_2$) at pH 2.7, to yield the selective precipitation of aluminum hydroxides and $CaSO_4$, followed by the addition of NaOH to reach pH 3.2. The result is a precipitate rich in iron, referred to herein as acicular goethite nanoparticles (AGNs). The AGN was washed multiple times with distilled water until the pH of the washing water became constant (pH = 4.0), it was filtered through a cellulose membrane in a press filter, dried at 90 °C for 5 h and stored for further use.

2.2 AGN characterization

The point of zero charge (pH_{pzc}) of the AGNs was measured used two methods. In the first method, 50 mL of NaCl 0.01 mol L^{-1} were placed in Erlenmeyer bottles and appropriate amounts of HCl or NaOH were added to obtain pH values between 2 and 12. AGNs (0.15 ± 0.01 g) were added to each bottle, subjected to agitation for 48 h and then filtered through a Buchner funnel with qualitative filter paper. The final pH of the filtrate was plotted against the initial pH and the pH at which the curve intercepted the line $pH_{initial} = pH_{final}$ was taken as the pH_{pzc}. The same procedure was repeated using a 0.1 mol L^{-1} NaCl solution. In the second method, 1.00 ± 0.01 g of AGNs were placed in 50 mL Erlenmeyer flasks and 20 mL of distilled water (free of CO_2) were then added. The bottles were placed under constant stirring for 24 h (shaker Dist, DI 951) and filtered through a Buchner

140 funnel with qualitative filter paper. The final pH was measured with a pH meter
141 (Micronal, model B474) and this was regarded as the pH_{pzc}.

142 The porosity and specific surface area of the AGNs were measured in a Quantachrome
143 Autosorb-1C nitrogen adsorptometer, via nitrogen adsorption and desorption at 77 K. The
144 total surface area was calculated from the adsorption isotherm using the BET equation [21].
145 The pore size distribution was obtained from the desorption isotherm following the BJH
146 method [22]. Micropore analysis was carried out by the SF method [23]
147 Microscopic images and the elemental composition of the AGNs were obtained using a
148 scanning electron microscope (JEOL JSM-6390LV) equipped with an energy dispersive X-
149 ray spectrometer (EDS). For the preparation of the AGNs, a small amount of powder was
150 added to acetone and the mixture was sonicated to disperse the particles. A small drop of
151 the suspension was placed on a clean polished flat surface (stub) and observed.
152 Alternatively, before analysis, the sample was coated with a thin layer of gold using a Leica
153 SCD 500 microsystem.
154 The crystalline structure of AGN particles was observed on an X'Pert Philips diffractometer
155 (XRD), with an angular range of 10-70° (2θ), CuKα radiation (λ = 1.5418 Å) and operating
156 at 40 kV and 30 mA.
157 Fourier transform infrared spectroscopy (FTIR) was carried out on an ABB Bomem
158 spectrometer (model FTLA 2000) in the range of 4000-400 cm^{-1} with the sample prepared
159 in KBr pellets.
160 Thermogravimetric analysis (TGA) and differential thermal analysis (DTA) were obtained
161 on a Shimadzu thermogravimetric analyzer (Model TGA/DTG-60) in the temperature range
162 of 25-900 ºC with a rate of 10 ºC min^{-1} under synthetic air atmosphere, with a flow rate of
163 100 mL min^{-1}.

164

165 2.3 Adsorption experiments

166 All glassware used in the experiment was washed with HCl to eliminate any interference
167 and then extensively washed with Milli-Q ultrapure water and dried.

168 *Adsorption kinetics*

169 The kinetics of adsorption of the standard reagents of humic acids (HAs) and phosphate on
170 AGNs was investigated. The aqueous solutions of HAs were prepared by diluting a
171 concentrated standard solution (Hümas-TKİ; pH 11-13, 12% (w/w humic + fulvic)) with
172 distilled water. The concentration of total organic carbon (TOC) in the HAs solutions was
173 determined with a TOC analyzer (Shimadzu, TOC-Analyzer TOC VCPH). Phosphate
174 solutions were prepared dissolving the KH_2PO_4 powder (Nuclear, ≥ 98% purity) in distilled
175 water and the final concentration was measured photometrically in a spectrophotometer
176 (Hach, DR 5000) using the amino acid method (method 8178; Hach Procedures Manual),
177 with a reading range of 0.23 to 30.00 mg L^{-1} PO_4^{3-}. The methodology was adapted from
178 Standard Methods for the Examination of Water and Wastewater [24]. Samples with a
179 concentration higher than 30.00 mg L^{-1} were diluted and the dilution factor was used to
180 calculate the concentration of the sample.

181 Constant volumes of standard solutions of HAs or phosphate at concentrations of 200 and
182 70 mg.L^{-1}, respectively, were added to fixed concentrations of AGNs (5.0 g.L^{-1}). The
183 solutions were shaken at 25.0 ± 1.0 °C for predetermined times, and then filtered through
184 PVDF membranes (Millipore) with diameters of 0.45 μm (HAs) and 0.22 μm (phosphate).
185 The TOC and phosphate concentrations of the solution were monitored before and after the
186 adsorption process. The kinetic results were fitted to the pseudo-first order or Lagergren
187 (Eq. 1) and pseudo-second-order (Eq. 2) models:

188 $$\log(q_e - q_t) = \log q_e - \frac{k_1}{2,303} t \quad (1)$$

189 $$\frac{t}{q_t} = \frac{1}{k_2 q_e^2} + \frac{1}{q_e} t \quad (2)$$

190 where k_1 (min^{-1}) and k_2 are the adsorption rate constants of the pseudo-first and pseudo-
191 second-order models (g mg^{-1} min^{-1}), respectively, and q_t, q_e are the amounts adsorbed at
192 time t and at equilibrium (mg g^{-1}) [25].

193

194 *Adsorption isotherms*

195 *Phosphate*: To assess the degree of affinity of the AGN sample with phosphate species, a
196 stock solution of KH_2PO_4 at a concentration of 1000 mg L^{-1} was prepared by dilution in
197 distilled water. The working solutions were prepared at the desired concentrations by
198 dilution from the stock solution. Batch experiments were carried out by adding a constant
199 mass of AGNs (0.500 ± 0.001 g) and varying the volume of phosphate solution of known
200 concentration (≈70 mg L^{-1} PO_4^{3-}) to obtain adsorbent concentrations ranging from 1.25 to
201 10.0 g L^{-1}. The flasks with solutions at different concentrations were capped, agitated in a
202 shaker for 70 h at 25.0 °C ± 1.0 °C and filtered through a PVDF membrane (0.22 μm,
203 Millipore). Before and after adsorption, the PO_4^{3-} (mg L^{-1}) concentrations of the samples
204 were measured photometrically according to the amino acid method, as described
205 elsewhere.

206 *HA*: Batch experiments were carried out to study the HA adsorption onto the AGN surface.
207 Varying amounts of a standard HA solution (200 mg L^{-1} TOC) were placed in contact with
208 a constant mass of AGNs (0.500 ± 0.001 g) in order to obtain adsorbent concentrations
209 ranging from 2.50 to 25.00 g L^{-1}. The flasks with solutions at different concentrations were
210 capped, agitated in a shaker for 52 h at 25.0 °C ± 1.0 °C, filtered through a PVDF membrane
211 (0.45 μm, Millipore) and the remaining TOC concentration was measured in a TOC
212 analyzer.

213 *Arsenate:* Aqueous solutions of As(V) at the desired concentration were prepared by
214 dilution from a 1000 mg L^{-1} As(V) stock solution made by dissolving sodium arsenate
215 dibasic heptahydrate $Na_2HAsO_4 .7H_2O$ (Sigma, ≥ 98% purity) in Milli-Q ultrapure water.
216 Different volumes of As(V) solution of known concentration (≈400 mg.L^{-1}) were placed in
217 contact with a constant mass of AGNs (0.50 ± 0.001 g) to obtain adsorbent concentrations
218 ranging from 1.25 to 16.67 g L^{-1}. After 24 h of agitation in a shaker (Dist, DI 951) at 25.0 ±
219 1.0 °C, the solutions were filtered through a 0.22 μm PVDF (Millipore) membrane and
220 analyzed by mass spectrometry with an inductively coupled plasma source (ICP-MS; Perkin
221 Elmer, Model NexION 300D, Shelton-USA), with sample introduction by pneumatic
222 nebulization.

223 For all adsorbates studied, control samples (without the addition of AGNs) were subjected
224 to the same conditions of temperature, contact time and analysis. In all cases, the pH of the
225 solution was not modified. The tests were carried out in triplicate. The amount of adsorbate
226 q_e (mg g^{-1}) adsorbed onto the AGN at equilibrium was calculated from the difference
227 between the initial C_o (mg L^{-1}) and the equilibrium C_e (mg L^{-1}) concentrations of each
228 species in solution (Equation 3):

229 $$q_e = \frac{(C_o - C_e)V}{w} \quad (3)$$

230 where V (L) is the volume of fluid and w is the mass of adsorbent (g).
231 The amount of each compound adsorbed onto the AGNs were described by the Langmuir
232 (Equation 4) and Freundlich (Equation 5) isotherm models:

233 $$q_e = \frac{b\, q_m C_e}{1 + bC_e} \quad (4)$$

234 $$q_e = K_F C_e^{1/n} \quad (5)$$

where q_m is the monolayer adsorption capacity (mg g^{-1}), b is the Langmuir constant (L mg^{-1}) [26]; and K_F and n (dimensionless) are the empirical Freundlich parameters. A high K_F value is ascribed to the system adsorbent-adsorbate when the adsorbate has a higher affinity towards the binding sites, while the constant n is proportional to the intensity of the reaction [27].

3. Results and discussion

3.1 AGN characterization

Table 1 shows the elemental composition, the point of zero charge (pH_{pzc}) in water and in NaCl brines, and the textural characteristics of the AGNs. The AGN contained approximately 80% iron (mass) and other elements such as C, Si, Ca and Al. These impurities represent less than ten percent (weight) of the material and are common in mine tailings. According to the Duncan test (5% significance level) there were insignificant differences between the pH_{pzc} values under the studied conditions. Thus, the surface of AGN is negatively charged at solution pH higher than 3.7, favoring the adsorption of cationic species, while the adsorption of anionic species may be favored at pH < pH_{pzc}. High purity synthetic goethite has a pH_{pzc} of approximately 9.0 [12], while natural iron oxides have a much lower PZC because of the presence of impurities. Surface-adsorbed anionic species such as CO_3^{2-} or SO_4^{3-} can significantly reduce the surface charge, whereas the adsorption of cationic substances such as Cu^{2+} or Zn^{+} increases the surface charge. The relatively high amount of carbon inpurity present in the samples investigated can be attributed to the presence of carbonates, which can reduce the pH_{pzc} [12].

The AGNs presented a reversible, type II, adsorption isotherm (S-shaped or sigmoid), which is associated to non-porous or macroporous adsorbents (data not shown) and unrestricted monolayer-multilayer adsorption. No hysteresis was observed, which is characteristic of the

absence of mesopores. The BET surface area and other textural characteristics obtained from the isotherm are shown in Table 1. BET surface area of synthetic goethites are commonly found in the range 11 to 153 $m^2 g^{-1}$ [12], by rigorous controlling the experimental conditions. The relatively large surface area of the AGNs used in this study is significant, considering that they were produced on an industrial scale where control over the synthesis conditions is much more difficult to achieve.

Table 1

Figure 1 shows the infrared spectrum for the AGNs recovered from the AMD. Bands that characterize the sludge recovered as goethite (α-FeOOH) are: 3431.67 and 3169.78 cm^{-1} due to O-H stretching; 630.68 cm^{-1} typical of Fe-O stretching; and 794.61 and 893.94 cm^{-1} due to in and out of plane OH vibrations, respectively [12].

Figure 1

Figure 2a shows the X-ray diffractogram of the solid recovered from the AMD. The diffraction patterns contain the diffraction lines of α-FeOOH (PDF card 29-0713), in a typical pattern as reported in the literature [28, 29] for synthetic goethite.

The crystal size was calculated from the Scherrer equation [30] ($L = k \lambda / B \cos\theta$), where k is a shape factor of the particle (equal to 1 for spherical particle, but the more common value of 0.9 was used), L is the crystal length in the direction of the d spacing, and λ and θ are the

284 wavelength and incident angle of the X-rays, respectively, and B is the line width at half
285 maximum (B) of the peak at (2θ = 21.3°, Figure 2a). The crystallite size of the AGNs was
286 found to be 23 nm, confirming that the recovered sludge can be characterized as goethite
287 nanosized. The morphology of the goethite crystallites (Figure 2b) shows needle-like or
288 acicular particles.

289

290 Figure 2

291 Figure 3 shows the TGA/DTA curves for the AGNs. The first weight loss step (≈ 2.5%) is
292 attributed to the evaporation of the free water in the powder. The subsequent weight loss of
293 11%, observed at 266.6 ºC results from the dehydroxylation (–OH) and the crystal transition
294 of goethite to hematite (α-Fe_2O_3). The last step change at 706.1 °C is due to the
295 transformation of hematite to magnetite (Fe_3O_4) [31], with a weight loss of around 1%.

296

297 Figure 3

298 3.2 Adsorption kinetics

299 The sorption kinetics was investigated to determine the adsorption rates for the phosphate
300 and humic acid solutions. The pseudo-first-order model did not fit the data for the adsorption
301 of humic acid and phosphate onto AGNs. However, the pseudo-second-order model
302 effectively described the behavior of both adsorbates, as shown in Table 2 by the higher
303 determination coefficient (R). This empirical model has no physical meaning, but it is
304 widely cited in the literature by several authors [27, 32, 33] and provided a good fit in this
305 study.

306

307 Table 2

Figure 4 shows the adsorption of phosphate and humic acid onto the AGNs over time and the fitting of the results by the pseudo-second-order model. Both phosphate and HAs showed similar kinetic behaviors. After 30 min of contact with the solid, around 65% of the initial concentration was adsorbed. The adsorbates then show a second slower adsorption step. The HAs reached equilibrium first, showing a nearly constant concentration after 4 h of contact with the AGNs (93% adsorbed). On the other hand, after 10 hours in solution 90% of the phosphate ions were adsorbed, which reached 96% after 90 h (Figure 4).

Figure 4

The adsorption of phosphate is characterized by an initial very fast process, taking place at $t < 5$ min, which is followed by a slower process, taking place at $t > 5$ min. During the initial fast adsorption process, aqueous oxoanions bind directly to the surface goethite groups [34]. Different mechanisms could be involved when the adsorption rate is low, such as surface precipitation, intraparticle diffusion, pores diffusion and surface binding heterogeneity [35]. The mechanism depends on the morphological and textural properties of the goethite nanoparticles [34].

3.3 Adsorption isotherms

The Langmuir and Freundlich models were used to describe the adsorption isotherms, and the fitted parameters are shown in Table 3 for humic acid, phosphate and arsenate.

The R values shown in Table 3 indicate that the experimental results were best described by the Langmuir model for phosphate adsorption. In contrast, the adsorption of humic acids was best described by the Freundlich model. The adsorption behavior of the arsenate was described similarly by the two models, despite Mamindy-Pajany et al. [36] reported that

333 Langmuir model should be most suitable to describe the adsorption behavior of arsenate
334 onto a goethite surface due to the formation of a monolayer of arsenate.
335 Table 3
336
337 Figures 5 shows the means and standard deviations of the experimental isotherms and the
338 fitting of these models for phosphate, humic acid and arsenate, respectively, at 25 ºC. The
339 results for the adsorption parameters in Table 3 showed a higher q_m value (i.e., higher
340 adsorption capacity) for the HAs followed by arsenate and then phosphate. In this regard,
341 two factors appear to be important and can explain the higher adsorption capacity of HAs
342 compared to the other adsorbates studied: a high molecular weight and the large number of
343 active sites available, consisting mainly of carboxyl and hydroxyl functional groups [37].
344 However, Kang and Xing [38] reported that the relatively small molecular weight HA
345 fractions had a greater affinity for the goethite surface, which contrast to other studies in
346 literature.
347 Figure 5
348 The surface properties of iron oxide are key factors in the adsorption process. Both arsenate
349 and phosphate can form an inner sphere of monodentate or bidentate–binuclear complexes
350 with iron oxides, which can be explained by the similar chemical structures of arsenates and
351 phosphates [39, 40]. This makes it difficult to explain the slightly higher affinity of the
352 adsorbent for arsenate than phosphate The nature of the surface complexation (monodentate
353 vs. bidentate, inner-sphere vs. outer-sphere) or the influence of other elements present on
354 the surface of AGNs, such as Ca and Al, may influence the degree of affinity [39]. So, to
355 fully explain these findings further studies are required.
356 Table 4 shows a comparison of the adsorption capacity results for the adsorbent investigated
357 in this study with other iron oxide adsorbents reported in the literature. The results obtained

with the AGNs recovered from AMD described herein are comparable with those obtained from synthetic, commercial or natural goethite. Many factors could contribute to the differences in the adsorption capacities observed in Table 4, including the sorbent surface area, the number of active sites available for adsorption, the iron content and the presence of impurities. Also, in the case of humic acids the molecular composition should be considered. Commercial HAs, for example, can differ significantly from natural organic matter present in natural environments, having a higher molecular weight, higher aromaticity and lower oxygen content than, for example, aquatic HAs and FAs. Goethite has a higher sorption affinity for high polar carboxylic functional moieties compared with low polarity carbohydrate and nonpolar aliphatic fractions [38], and the amount of these molecular groups present is dependent on the origin of the HAs.

Another important aspect for the adsorption of arsenate, phosphate and humic acid is the size and degree of aggregation of the iron oxides particles. A decrease in the particle size from 300 to 12 nm of the size of nanocrystalline magnetite particles was found to increase the adsorption capacity of As^{3+} and As^{5+} by approximately 200 times [41]. Interestingly, this increase is greater than that expected based simply on considering the increase in surface area with smaller particles and suggests that the mechanisms associated with the sorption of arsenate by nanoscale iron oxide materials differs from that of bulk systems, and is somewhat affected by the aggregation of the nanoparticles. The AGNs used in this study were in the upper range (average particle size 67 x 430 nm (diameter x lenght)) and therefore further optmization of the industrial process for recovery of AGNs from AMD may lead to an increase of the adsoption capacity of these AGNs.

Table 4

382 The results obtained in this study (Table 4) indicate that the AGNs recovered from an
383 industrial scale from acid mine drainage sludge have great potential for a wide range of
384 applications to treat waters contamined with arsenate, phosphate or humic acid contributing
385 to adding a high value to the waste generated from coal mining.
386
387
388 **4. Conclusions**
389 In this study, sludge resulting from the AMD treatment process in a coal mine in southern
390 Brazil, precipitated on an industrial scale, was characterized and tested for its capacity to
391 adsorb the pollutants humic acids, arsenate and phosphate in aqueous solution. The SEM,
392 XRD, FTIR, and TGA/DTA results indicated the presence of around 80% iron in the sample
393 corresponding to the mineral goethite in the form of acicular nanoparticles with a large
394 specific surface area (102 m^2 g^{-1}).
395 The pseudo-second-order model effectively describes the kinetic behavior of the adsorption
396 of humic acids and phosphate onto the acicular goethite nanoparticles (AGNs). Phosphate
397 and HAs have similar kinetic behaviors, with a rapid adsorption step followed by a slow
398 step. The experimental adsorption results were best described by the Langmuir model for
399 phosphate and by the Freundlich model for humic acids. The adsorption behavior for
400 arsenate was described similarly by both models. The highest adsorption capacity was
401 obtained for HAs (37.30 ± 2.19 mgC g^{-1}), followed by arsenate (19.91 ± 5.51 mg As(V) g^{-1})
402 and finally phosphate (12.98 ± 0.15 mgPO_4^{3-} g^{-1}). This study has shown a good prospect
403 for the valorization of the AGNs product derived at industrial scale from the acid mine
404 drainage slurry waste arising from the mining of coal.
405
406 **Acknowledgements**

The authors are grateful to the Brazilian governmental agency the National Council for Technological and Scientific Development (CNPq, Brazil) for financial support and Carbonífera Criciúma for providing the AMD sludge.

References

[1] Madeira, V.S. (2010). Coal mine residues usage for the production of high value added products. Doctor degree thesis, Chemical Engineering Department, Federal University of Santa Catarina, Florianópolis-SC, Brazil. *(In Portuguese).*

[2] Prasad, B.; Mortimer, R.J.G. (2011). Treatment of acid mine drainage using fly ash zeolite. *Water Air Soil Pollut*, 218: 667 – 679.

[3] Sarmiento, A.M.; DelValls, A.; Nieto, J.M.; Salamanca, M.J.; Caraballo, M.A. (2011). Toxicity and potential risk assessment of a river polluted by acid mine drainage in the Iberian Pyrite Belt (SW Spain). *Science of the Total Environment*, 409: 4763 – 4771.

[4] Cheng, S.; Jang, J.-H.; Dempsey, B.A.; Logan, B.E. (2011). Efficient recovery of nano-sized iron oxide particles from synthetic acid-mine drainage (AMD) water using fuel cell technologies. *Water Research*, 45: 303-307.

[5] Bogush, A. A.; Voronin, V.G. (2011). Application of a peat-humic agent for treatment of acid mine drainage. *Mine Water and the Environment*, 30: 185 – 190.

[6] Buzzi, D.C.; Viegas, L.S.; Silvas, F.P.C.; Espinosa, D.C.R.; Rodrigues, M.A.S.; Bernardes, A.M.; Tenório, J.A.S. (2011). The use of microfiltration and electrodialysis for treatment of acid mine drainage. IMWA Proceedings. In: "*11th International Mine Water Association Congress – Mine Water – Managing the Challenges"* p. 287 – 291 Aachen, Germany.

[7] Johnson, D.B.; Hallberg, K.B. (2005). Acid mine drainage remediation options: a review. *Science of the Total Environment*, 338: 3 – 14.

[8] Kirby, C.S.; Decker, S.M.; Macander, N.K. (1999). Comparison of color, chemical and mineralogical compositions of mine drainage sediments to pigment. *Environmental Geology*, 37(3): 243 – 254.

434 [9] Kairies, C.L.; Capo, R.C.; Watzlaf, G.R. (2005). Chemical and physical properties of
435 iron hydroxide precipitates associated with passively treated coal mine drainage in the
436 Bituminous Region of Pennsylvania and Maryland. *Applied Geochemistry*, 20(8): 1445 –
437 1460.
438 [10] Cui, M.; Jang, M.; Cho, S-H.; Khim, J. (2011). Potential application of sludge produced
439 from coal mine drainage treatment for removing Zn(II) in an aqueous phase. *Environmental*
440 *Geochemistry and Health*, 33(suppl. 1): 103 – 112.
441 [11] Rait, R.; Trumm, D.; Pope, J.; Craw, D.; Newman, N.; MacKenzie, H. (2010).
442 Adsorption of arsenic by iron rich precipitates from two coal mine drainage sites on the
443 West Coast of New Zealand. *New Zealand Journal of Geology and Geophysics*, 53(2-3):
444 177 – 193.
445 [12] Cornell, R.M.; Schwertmann, U. (2003) *The iron oxides: structure, properties,*
446 *reactions, occurrences and uses.* 2nd ed. Weinheim: Willey-VCH.
447 [13] Andersen, S.L.F.; Flores, R.G.; Madeira, V.S.; José, H.J.; Moreira, R.F.P.M. (2012)
448 Synthesis and characterization of acicular iron oxide particles obtained from acid mine
449 drainage and their catalytic properties in toluene oxidation, *Ind. Eng. Chem. Res*., 51 (2):
450 767–774.
451 [14] Flores, R. G.; Andersen, S.L.; Maia, L.K.; José, H.J.; Moreira, R.F.P.M. (2012)
452 Recovery of iron oxides from acid mine drainage and their application as adsorbent or
453 catalyst, *J. Environ. Management*, 111: 53-60.
454 [15] Carabante, I.; Grahn, M.; Holmgren, A.; Hedlund, J. (2010). In situ ATR–FTIR studies
455 on the competitive adsorption of arsenate and phosphate on ferrihydrite. *Journal of Colloid*
456 *and Interface Science*, 351: 523 – 531.
457 [16] Hopenhayn, C. (2006). Arsenic. In: Arsenic in drinking water: impact on human health.
458 *Elements*, 2 (2), 103 – 107.

459 [17] Benyoucef, S.; Amrani, M. (2011). Adsorption of phosphate ions onto low cost Aleppo
460 pine adsorbent. *Desalination*, 275: 231 – 236.
461 [18] Ho, J. C.; Michalak, A. M. (2015). Challenges in tracking harmful algal blooms: A
462 synthesis of evidence from Lake Erie, *Journal of Great Lakes Research*, 41(2): 317-325.
463 [19] Zach-Maor, A.; Semiat, R.; Shemer, H. (2011). Fixed bed phosphate adsorption by
464 immobilized nano-magnetite matrix: experimental and a new modeling approach.
465 *Adsorption*, 17(6): 929 – 936.
466 [20] Daifullah, A.A.M.; Girgis, B.S.; Gad, H.M.H. (2004). A study of the factors affecting
467 the removal of humic acid by activated carbon prepared from biomass material. *Colloids*
468 *and Surfaces A: Physicochem. Eng. Aspects,* 235: 1–10.
469 [21] Brunauer, S.; Emmett, P.H.; Teller, E. (1938). Adsorption of gases in multimolecular
470 layers. *Journal of American Chemical Society*, 60: 309 - 319.
471 [22] Barret, E.P.; Joyner, L.G.; Halenda, P.P. (1951). The determination of pore volume and
472 area distributions in porous substances. I. Computations from nitrogen isotherms. *Journal*
473 *of American Chemical Society*, 73(1): 373 – 380.
474 [23] Saito, A.; Foley, H.C. (1991). Curvature and parametric sensitivity in models for
475 adsorption in micropores. *AIChE Journal*, 37(3): 429 – 436.
476 [24] APHA, *Standard Methods for the Examination of Water and Wastewater*. 2012. 22nd
477 Edition.
478 [25] Gu, B.; Schmitt, J.; Chen, Z.; Liang, L.; McCarthy, J. (1995). Adsorption and
479 desorption of different organic matter fractions on iron oxide. *Geochimica et Cosmochimica*
480 *Acta*, 59(2), 219 – 229.
481 [26] Hsieh, C-T.; Teng, H. (2000). Langmuir and Dubinin–Radushkevich analyses on
482 equilibrium adsorption of activated carbon fabrics in aqueous solutions. *Journal of*
483 *Chemical Technology and Biotechnology*, 75(11): 1066 – 1072.

484 [27] D'Arcy, M.; Weiss, D.; Bluck, M.; Vilar, R. (2011). Adsorption kinetics, capacity and
485 mechanism of arsenate and phosphate on a bifunctional TiO_2–Fe_2O_3 bi-composite. *Journal*
486 *of Colloid and Interface Science*, 364(1): 205 – 212.
487 [28] Brigante, M.; Zanini, G.; Avena, M. (2010). Effect of humic acids on the adsorption of
488 paraquat by goethite. *Journal of Hazardous Materials*, 184(1-3): 241 – 247.
489 [29] Rong, S.; Yongfeng, J.; Chengzhi, W. (2009). Competitive and cooperative adsorption
490 of arsenate and citrate on goethite. *Journal of Environmental Sciences*, 21: 106 – 112.
491 [30] Hall, B.D.; Zanchet, D.; Ugarte, D. (2000). Estimating nanoparticle size from
492 diffraction measurements. *Journal of Applied Crystallography*, 33(6): 1335 – 1341.
493 [31] Yaoxing, H.; Xinsheng, M.; Hongming, C.; Haiying, Z.; Qiufang, W. (2004).
494 Morphological study and thermal analysis of surface modified α-FeOOH via in situ
495 polymerization of methyl methacrylate. *Materials Research Bulletin*, 39: 1159 – 1166.
496 [32] Zhong-liang, S.; Fu-me, L.; Shu-hua, Y. (2011). Adsorptive removal of phosphate from
497 aqueous solutions using activated carbon loaded with Fe(III) oxide. *New Carbon Materials*,
498 26(4): 299 – 306.
499 [33] Song, X.; Pan, Y.; Wu, Q.; Cheng, Z.; Ma, W. (2011). Phosphate removal from aqueous
500 solutions by adsorption using ferric sludge. *Desalination*, 280(1-3): 384 – 390.
501 [34] Strauss, R.; Brummer, G.W.; Barrow, N.J. (1997). Effects of crystallinity of goethite:
502 II. Rates of sorption and desorption of phosphate. *European Journal of Soil Science*, 48(1):
503 101 -114.
504 [35] Luengo, C.; Brigante, M.; Avena, M. (2007). Adsorption kinetics of phosphate and
505 arsenate on goethite. A comparative study. *Journal of Colloid and Interface Science*, 311(2):
506 354 – 360.

507 [36] Mamindy-Pajany, Y.; Hurel, C.; Marmier, N.; Romeo, M. (2011). Arsenic (V)
508 adsorption from aqueous solution onto goethite, hematite, magnetite and zero-valent iron:
509 Effects of pH, concentration and reversibility. *Desalination*, 281(1): 93 – 99.
510 [37] Weng, L.; Van Riemsdijk, W.H.; Koopal, L.K.; Hiemstra, T. (2006). Adsorption of
511 humic substances on goethite: comparison between humic acids and fulvic acids.
512 *Environmental Science & Technology*, 40(24): 7494 – 7500.
513 [38] Kang, S.; Xing, B. (2008). Humic acid fractionation upon sequential adsorption onto
514 goethite. *Langmuir*, 24: 2525 - 2531.
515 [39] Gao Y.; Mucci A. (2001). Acid base reactions, phosphate and arsenate complexation,
516 and their competitive adsorption at the surface of goethite in 0.7 M NaCl solution.
517 *Geochimca et Cosmochimica Acta*, 65: 2361–2378.
518 [40] Fendorf, S.; Eick, M.J.; Grossl, P.; Sparks, D.L. (1997). Arsenate and chromate
519 retention mechanisms on goethite. 1. Surface structure. *Environmental Science and*
520 *Technology*, 31: 315 – 320.
521 [41] Mayo, J.T.; Yavuz, C.; Yean, S.; Cong, L.; Shipley, H.; Yu, W.; Falkner, J.; Kan, A.;
522 Tomson, M.; Colvin, V.L. (2007). The effect of nanocrystalline magnetite size on arsenic
523 removal. *Science and Technology of Advanced Materials*, 8(1-3): 71 – 75.
524 [42] Matis, K.A.; Zouboulis, F.B.; Malamas, M.D.; Alfonso, M.D.R.; Hudson, M.J. (1997).
525 Flotation removal of As(V) onto goethite. *Environmental Pollution*, 97(3): 239 – 245.
526 [43] Dixit, S.; Hering, J. (2003). Comparison of arsenic (V) and arsenic (III) sorption onto
527 iron oxide minerals: implications for arsenic mobility. *Environmental Science and*
528 *Technology*, 37(18): 4182 – 4189.
529 [44] Lehmann, M.; Zouboulis, A.I.; Matis, K.A.; Grohmann, A. (2005). Sorption of arsenic
530 oxyanions from aqueous solution on goethite: study of process modeling. *Microchimica*
531 *Acta*, 151(3-4): 269 – 275.

[45] Giménez, J.; Martínez, M.; Pablo, J.; Rovira, M.; Duro, L. (2007). Arsenic sorption onto natural hematite, magnetite, and goethite. *Journal of Hazardous Materials*, 141(3): 575 – 580.

[46] Asta, M.P.; Cama, J. ; Martínez, M.; Giménez, J. (2009). Arsenic removal by goethite and jarosite in acidic conditions and its environmental implications. *Journal of Hazardous Materials*, 171(1-3): 965 – 972.

[47] Saito, T.; Koopal, L.K.; van Riemsdijk, W.H.; Nagasaki, S.; Tanaka, S. (2004). Adsorption of humic acid on goethite: isotherms, charge adjustments and potential profiles. *Langmuir*, 20(3): 689 – 700.

[48] Antelo, J.; Arce, F.; Avena, M.; Fiol, S., López, R.; Macías, F. (2007) Adsorption of a soil humic acid at the surface of goethite and its competitive interaction with phosphate. *Geoderma*, 138(1-2): 12 – 19.

[49] Juang, R-S.; Chung, J-Y. (2004). Equilibrium sorption of heavy metals and phosphate from single-and binary-sorbate solutions on goethite. *Journal of Colloid and Interface Science,* 275(1): 53 – 60.

[50] Chitrakar, R.; Tezuka, S.; Sonoda, A.; Sakane, K.; Ooi, K.; Hirotsu, T. (2006). Phosphate adsorption on synthetic goethite and akaganeite. *Journal of Colloid and Interface Science*, 298: 602 - 608.

[51] Xie, J.-J.; Qing, C.,-S.; Chen, T.-H.; Guo, Y.; Pan, M. (2007). Comparison of phosphate adsorption capacity among different iron hydroxides/oxides. *Yanshi Kuangwuxue Zazhi*, 26 (6): 535 - 538.

555 **Caption of Tables**

556

557 Table 1: Elemental composition, point of zero charge and textural characteristics of AGN.

558 Table 2: Parameters obtained from fitting of pseudo-first-order and pseudo second order

559 kinetic models for adsorption of phosphate and humic acids (HAs) from solutions.

560 Table 3: Langmuir and Freundlich fitted parameters for humic acids (HAs), phosphate and

561 arsenate at 25 ºC.

562 Table 4: Comparison of the adsorption capacities for the goethite adsorbent used in this

563 study and others reported in the literature.

564

Table 1: Elemental composition, point of zero charge and textural characteristics of AGN.

Element	Element weight and error (%) (dry basis)
Fe	79.43 ± 1.12
O	12.23 ± 0.27
C	6.32 ± 0.49
Si	1.14 ± 0.12
Ca	0.53 ± 0.09
Al	0.36 ± 0.07
***Point of zero charge (pH_{pzc})**	
H_2O	3.55 ± 0.15[a]
NaCl 0.01 mol.L^{-1}	3.69 ± 0.28[a]
NaCl 0.1 mol.L^{-1}	3.53 ± 0.19[a]
Textural characterization	
BET surface area ($m^2.g^{-1}$)	102.1
Total pore volume ($cm^3.g^{-1}$)	0.256
Micropore volume ($cm^3.g^{-1}$)	0.036
Micropore diameter (nm)	9.64

565 *Averages followed by different superscript letters in the same column are statistically different, according to the Duncan test.

566

567

Table 2: Parameters obtained from fitting of pseudo-first-order and pseudo second-order kinetic models for adsorption of phosphate and humic acids (HAs) from solutions.

Adsorbate	Pseudo-first order kinetic model			Pseudo-second order kinetic model			
	k_1 (min^{-1})	q_1 ($mg.g^{-1}$)	R	k_2 ($g.mg^{-1}.min^{-1}$)	q_2 ($mg.g^{-1}$)	h ($mg.g^{-1}.min^{-1}$)	R
HAs	$4.84x10^{-3}$	7.25	0.745	$2.31x10^{-3}$	27.40	1.74	0.999
Phosphate	$9.21x10^{-4}$	3.14	0.901	$2.62x10^{-3}$	12.97	0.44	0.999

568

569

570

Table 3: Langmuir and Freundlich fitted parameters for humic acids (HAs), phosphate and arsenate at 25 °C.

	Langmuir			Freundlich		
	q_m (mg.g^{-1})	b (L.mg^{-1})	R^2	K_F	n_F	R^2
Phosphate	12.98 ± 0.15	3.69 ± 0.38	0.997	9.19 ± 0.46	10.18 ± 0.02	0.985
HAs	37.30 ± 2.19	0.15 ± 0.04	0.985	8.40 ± 0.92	2.65 ± 0.03	0.993
Arsenate	19.91 ± 5.51	0.03 ± 0.07	0.853	9.89 ± 15.33	9.76 ± 0.27	0.850

571

Table 4: Comparison of the adsorption capacities for the goethite adsorbent used in this study and others reported in the literature.

Adsorbate	Removal capacity	Mineral type	Reference
As (mg As(V).g^{-1})	0.45 to 45.52	Synthetic or commercial Goethite	[35, 41-45]
	12.0 to 74.0	Precipitated from AMD	[11]
	19.91	AGN from AMD	Present study
HAs (mgC.g^{-1})	10.79 to 97.13	Goethite	[36, 46, 47].
	3.75 to 5.71	Commercial Goethite	[37]
	37.30	AGN from AMD	Present study
PO_4^{3-} ($mgPO_4^{3-}$.g^{-1})	15.40 to 18.27	Goethite	[48]
	73.59	Goethite	[48]
	< 5.5	Goethite	[50]
	12.98	AGN from AMD	Present study

572

Caption of Figures

Figure 1: FTIR spectrum for AGNs recovery from AMD.

Figure 2: X-ray diffractogram (a) and SEM micrographs (b) of the AGN recovered from AMD.

Figure 3: DTA and TGA curves for the AGNs.

Figure 4: (a) Kinetics data for the removal of phosphate and humic acids (HAs) from solution by adsorption onto AGNs. (b) Fit for the pseudo-second-order model.

Figure 5: Langmuir and Freundlich models fitted to the adsorption isotherms obtained for the adsorption of phosphate (a), humic acids (b) and arsentate (c) onto AGNs at 25°C.

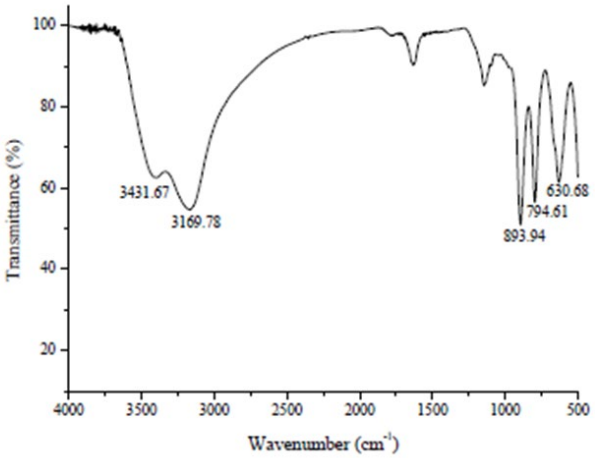

Figure 1: FTIR spectrum for AGNs recovery from AMD.

584

585

586

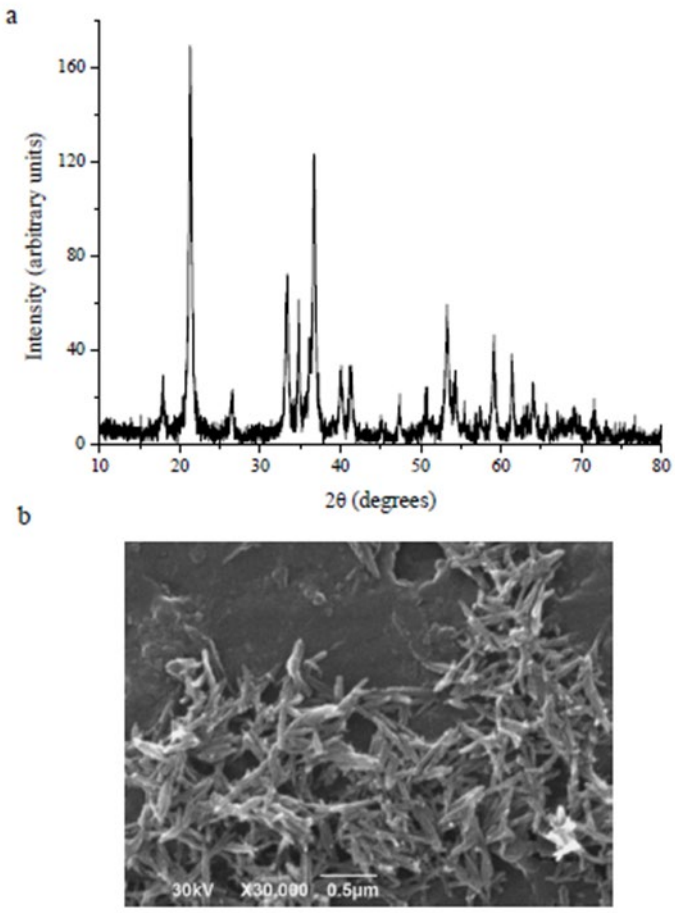

Figure 2: X-ray diffractogram (a) and SEM micrographs (b) of the AGN recovered from AMD.

587

588

589

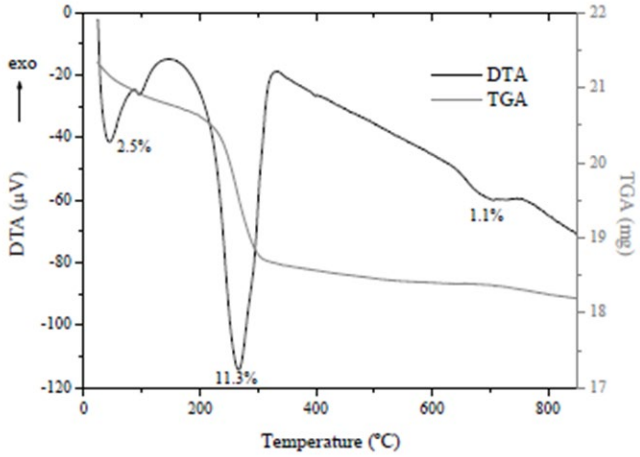

Figure 3: DTA and TGA curves for the AGNs.

590

591

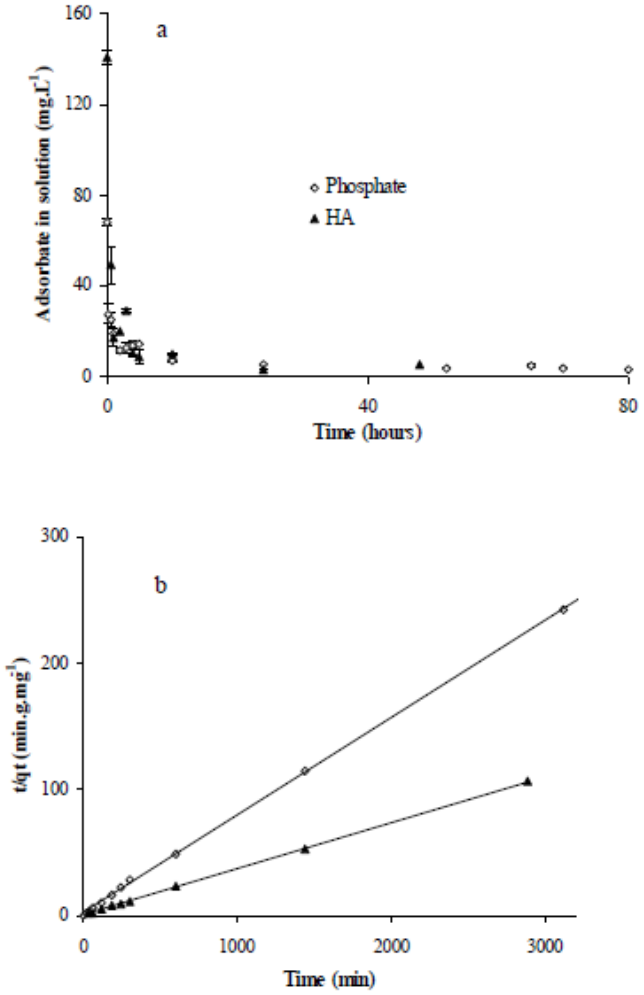

Figure 4: (a) Kinetics data for the removal of phosphate and humic acids (HAs) from solution by adsorption onto AGNs. (b) Fit for the pseudo-second-order model.

592

593

594

595

596

597

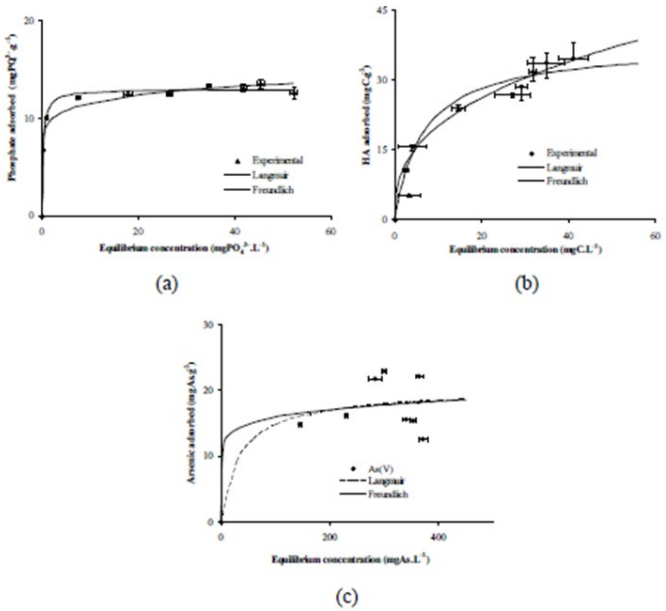

Figure 5: Langmuir and Freundlich models fitted to the adsorption isotherms obtained for the adsorption of phosphate (a), humic acids (b) and arsentate (c) onto AGNs at 25 °C.

598